

RF BREAKDOWN AND DARK CURRENT STUDIES IN SHORT-PULSE ACCELERATION

Gaurab Rijal, Michael Shapiro, Xueying Lu¹, Northern Illinois University, DeKalb, IL, USA

Scott Doran, John Power, Argonne National Laboratory, Lemont, IL, USA

¹also at Argonne National Laboratory, Lemont, IL, USA

Abstract

Recent experimental studies at the Argonne Wakefield Accelerator (AWA) have shown that operating RF cavities with short pulses of only a few nanoseconds in duration can raise the accelerating gradient to nearly 400 MV/m in a series of X-band structure tests. These results motivate further investigation into the breakdown physics underlying the short-pulse acceleration regime. In this work, we present analytical models and numerical simulations of dark current dynamics in X-band cavities driven by short RF pulses. These studies explore key phenomena associated with RF breakdown across various time scales. Building on these insights, we describe the design and experimental plan for a single-cell X-band RF cavity for high-power breakdown tests with short pulses. The cavity is designed to operate at 11.7 GHz and optimized for high-gradient operation with 6 ns long RF pulses and integrated with RF breakdown diagnostics. This work aims to deepen the understanding of RF breakdown physics in the short-pulse regime and to support the development of compact linear accelerators for future applications.

INTRODUCTION

The pursuit of a higher accelerating gradient is central to the development of compact linear accelerators for applications in medical therapy, industrial systems, and future high-energy physics experiments. In recent years short-pulse acceleration has emerged as a promising technique to mitigate RF breakdown and achieve gradients well beyond conventional limits. Specifically, operating RF cavities with nanosecond-scale pulse has demonstrated a significant reduction in breakdown probability while enabling a peak surface field exceeding 400 MV/m in X-band structures. Experimental work at Argonne Wakefield Accelerator (AWA) has shown that X-band cavities driven by a 6ns long RF pulse can sustain a much higher gradient [1–4]. These observations call for a deeper theoretical and experimental understanding of breakdown and dark-current dynamics in this short-pulse regime.

To investigate these effects, this paper first summarizes a study of dark current dynamics [5] in an existing X-band photocathode cavity [1]. Building on these insights, the second part of this paper introduces the design and experimental plan for a dedicated single-cell X-band cavity at 11.7 GHz, optimized for short-pulse operation and equipped with advanced RF diagnostics. Together, these efforts aim to understand the scaling laws and mechanisms that govern breakdown onset in short-pulse regime.

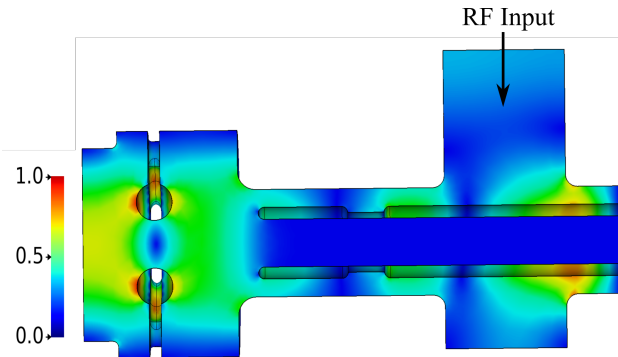


Figure 1: Normalized electric field distribution along the midplane of the X-band photogun cavity at 11.7 GHz, with peak field enhancement near the iris region.

DARK CURRENT STUDY IN AN X-BAND PHOTOCATHODE CAVITY

In this section, we present both electron trajectory analysis and particle-in-cell (PIC) simulations to study dark current dynamics in an X-band photocathode cavity. The cavity is a $1 + \frac{1}{2}$ -cell standing-wave structure, overcoupled to achieve a low loaded quality factor (Q_L) and a short RF filling time compatible with nanosecond-scale input pulses. The electric field distribution in the photocathode cavity is shown in Fig. 1. A comprehensive description of the design and high-power testing of the photocathode cavity is provided in [1]. To identify regions susceptible to dark current growth and multipacting, we begin by simulating the trajectories of field-emitted electrons launched from the iris under steady-state RF fields. Sample electron trajectories emitted from iris surface at electric field of 40 MV/m field is shown in Fig. 2(a). The resulting trajectories show that a majority of the emitted electrons impact the cavity sidewall.

To study multipacting behavior under the transient short-pulse operation, we performed CST PIC simulations using RF signals of different temporal profile. Secondary electron emission (SEE) was enabled on the sidewall surface of region I in the half-cell as shown in Fig. 2(b). Two RF input pulses were considered, as illustrated in Fig. 2(c): one with a 3 ns rise, 3 ns flat-top, and 3 ns fall, and another with a 30 ns rise. Seeding electrons were emitted from iris and simulation setup is consistent with method described in [6]. The simulation results are presented in Fig. 3, showing the on axis electric field (left axis) and the total number of multipacting electrons (right axis) over time. In the case of the 3–3–3 ns pulse [Fig. 3(a)], The observed multipacting peaks during both the rising and falling edges of the 3–3–3 ns pulse correspond to resonance orders $N = 1$ through 4.

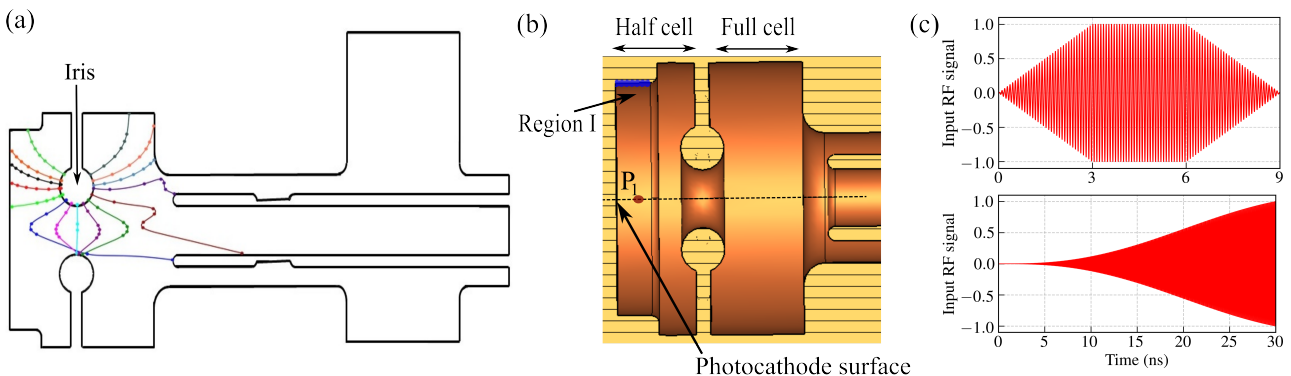


Figure 2: (a) Field-emitted electron trajectories from the iris surface at a static field of 40 MV/m; (b) CST PIC simulation setup to study multipacting, with the sidewall of Region I assigned secondary electron emission properties; (c) Two RF input pulse profiles used in the multipacting study. Top: short pulse with 3 ns rise, 3 ns flattop, and 3 ns fall. Bottom: long pulse with 30 ns rise.

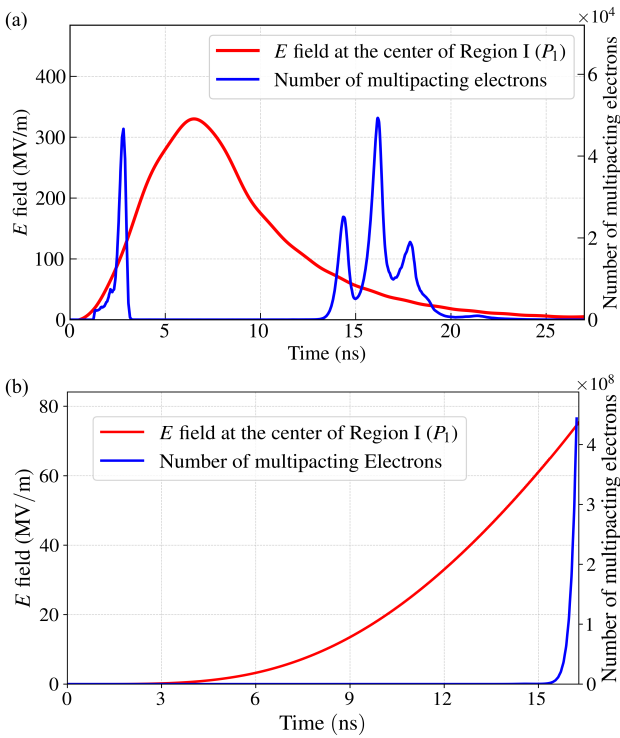


Figure 3: PIC simulation results comparing multipacting behavior under two RF input pulse shapes shown in Fig. 2. Each panel shows the electric field amplitude (left Y-axis) and the number of multipacting electrons (right Y-axis) as functions of time. (a) 3-3-3 ns pulse; (b) 30 ns pulse.

Sample resonance electron trajectories associated with these modes are provided in [5]. In contrast, the 30 ns rising pulse [Fig. 3(b)] exhibits a slower increase in electric field amplitude, which extends the duration over which the field remains within the multipacting-prone regime. This leads to a significantly higher accumulation of multipacting electrons, as sustained resonance conditions allow repeated wall collisions and secondary emissions. These observations underscore the critical sensitivity of multipacting behavior to the RF signal's length and temporal structure. Rapidly varying pulses limit the time window for electron multipli-

Table 1: Design Parameters of the 11.7 GHz Single-Cell X-Band Cavity

Parameter	Value
Beam aperture radius, a	1.76 mm
Loaded quality factor, Q_L	≈ 130
Shunt impedance, r_s	148 MΩ/m
Accelerating gradient, E_{acc}	$34 \sqrt{P_{\text{peak}} (\text{MW})} \text{ MV/m}$
$E_p/E_0 T$	1.65
$H_p Z_0 / E_0 T$	1.25
Cavity fill time, τ	6.86 ns

cation, whereas slowly ramped pulses promote sustained multipacting due to prolonged exposure to resonant field levels.

DESIGN OF SINGLE-CELL X-BAND CAVITY

To experimentally investigate RF breakdown and related phenomena under short-pulse conditions, a single-cell X-band cavity has been designed for operation at 11.7 GHz. The design is based on a symmetric re-entrant geometry.

Electromagnetic simulations were performed using CST Microwave Studio to optimize the RF performance of the cavity, with emphasis on maximizing the transient accelerating gradient (E_0) under short-pulse excitation, while minimizing peak surface electric field (E_p) and magnetic field (H_p). The resulting cavity parameters and RF figures of merit are summarized in Table 1.

The simulated S-parameters confirm the design frequency of 11.7 GHz, as shown in Fig. 4. A matching waveguide is designed to extract a small portion of the power from the standing-wave cavity for real-time RF diagnostics. The transmission coefficient from the input port to the matching waveguide port is $S_{21} = -40 \text{ dB}$. The optimized cavity structure is shown in Fig. 5. For fabrication, the cavity is split along the midplane into two halves. Each half will be machined from oxygen-free high-conductivity (OFHC) copper. After machining, the two halves will be brazed

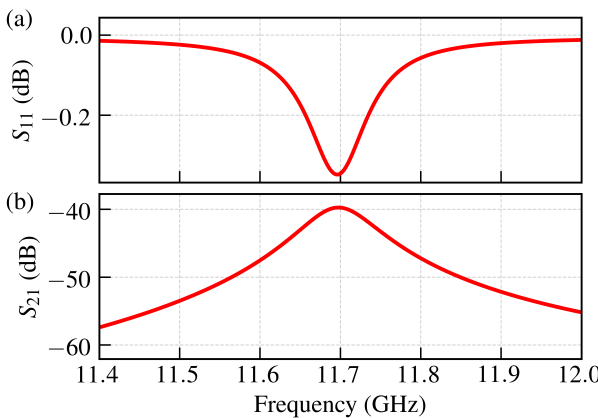


Figure 4: Simulated S-parameters of the X-band cavity.
(a) Reflection coefficient (S_{11}) (b) Transmission coefficient (S_{21}).

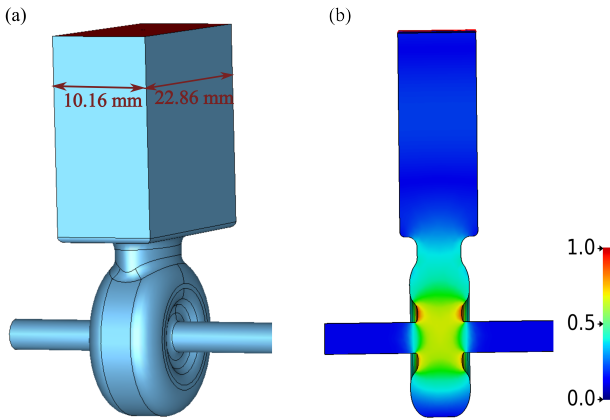


Figure 5: Design of the single-cell X-band cavity at 11.7 GHz. (a) Vacuum model of the cavity with the coupler to the WR90 waveguide. (b) Normalized electric field distribution on the midplane.

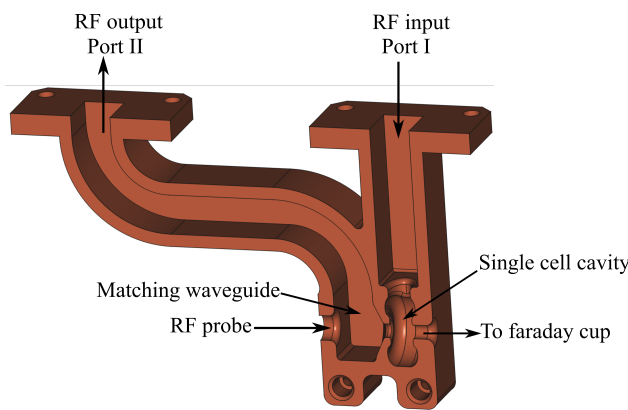


Figure 6: 3D model of one half of the cavity, split along the midplane.

to form a single structure. A 3D model of the split cavity structure is shown in Fig. 6.

The structure supports integration with time-resolved RF diagnostics and dark current detectors for breakdown characterization during short-pulse operation, including dark

current monitors (Faraday cups), measurements of transmitted and reflected RF signals from the waveguide ports, and an electric field probe. To enable detailed diagnostics of breakdown events and dark current emission, a Faraday cup will be positioned downstream along the beamline to collect dark current as directed in Fig. 6, while an RF pickup probe will be placed at the opposite end of the beam pipe. Directional couplers will be installed at the input and output ports to record the incident, reflected, and transmitted RF signals in real time. These measurements will allow detection of transient behaviors associated with breakdown, including dark current growth, abrupt field collapse and reflected power changes.

CONCLUSIONS

We have investigated the behavior of a high-gradient X-band photocathode cavity under short-pulse excitation through a combination of particle tracking and Particle-in-Cell (PIC) simulations. Starting from steady-state RF field distributions, we identified regions prone to dark current emission by launching electron trajectories from various locations within the cavity. To further examine multipacting phenomena, PIC simulations were performed under both short-pulse and long-pulse RF drive conditions. The results show that the temporal shape of the RF signal plays a critical role in multipacting dynamics: while long pulses lead to significant electron growth, short pulses—such as the 3–3–3 ns profile—effectively limit the number of multipacting electrons. These findings highlight the potential of RF pulse shaping as a strategy to mitigate dark current. To experimentally investigate these effects, a single-cell X-band cavity is designed for compatibility with nanosecond-scale RF pulses. The cavity supports high accelerating gradient and its design includes integrated diagnostics breakdown analysis. The cavity is currently under fabrication, with high-power testing and breakdown studies planned at AWA. These efforts aim to advance the understanding of RF breakdown in short-pulse regimes and inform the development of compact, high-gradient accelerator structures.

ACKNOWLEDGMENTS

This research was supported by the U.S. Department of Energy, Office of Science, Office of High Energy Physics under Award No. DE-SC0021928.

REFERENCES

- [1] W. H. Tan *et al.*, “Demonstration of sub-GV/m accelerating field in a photoemission electron gun powered by nanosecond X-band radio-frequency pulses”, *Phys. Rev. Accel. Beams*, vol. 25, no. 8, p. 083402, Aug. 2022.
doi:10.1103/PhysRevAccelBeams.25.083402
- [2] D. Merenich *et al.*, “Breakdown insensitive acceleration regime in a metamaterial accelerating structure”, *Phys. Rev. Accel. Beams*, vol. 27, no. 4, p. 041301, Apr. 2024.
doi:10.1103/PhysRevAccelBeams.27.041301

- [3] M. Peng *et al.*, “Generation of high power short RF pulses using an X -band metallic power extractor driven by high charge multi-bunch train”, in *Proc. IPAC’19*, Melbourne, Australia, Jun. 2019, pp. 734–737.
doi:10.18429/JACoW-IPAC2019-MOPRB069
- [4] S. Weatherly *et al.*, “Standing wave dielectric disk accelerating structure design and low power measurements”, *Nucl. Instrum. Methods Phys. Res. A: Accel. Spectrom. Detect. Assoc. Equip.*, vol. 1073, p. 170283, 2025.
doi:10.1016/j.nima.2025.170283
- [5] G. Rijal, M. Shapiro, and X. Lu, “Analytical and numerical studies of dark current in radiofrequency structures for short-pulse high-gradient acceleration”, *arXiv*, 2025.
doi:10.48550/arXiv.2507.04483
- [6] H. Xu, M. A. Shapiro, and R. Temkin, “Measurement of internal dark current in a 17 GHz, high gradient accelerator structure”, *Phys. Rev. Accel. Beams*, vol. 22, no. 2, p. 021302, Feb. 2019.
doi:10.1103/PhysRevAccelBeams.22.021302